International Journal of Concrete Structures and Materials
DOI 10.1007/s40069-017-0197-4
ISSN 1976-0485 / eISSN 2234-1315

Evaluation of Crack Propagation and Post-cracking Hinge-type Behavior in the Flexural Response of Steel Fiber Reinforced Concrete

Sahith Gali and Kolluru V. L. Subramaniam*

(Received July 28, 2016, Accepted March 23, 2017)

Abstract: An experimental evaluation of crack propagation and post-cracking behavior in steel fiber reinforced concrete (SFRC) beams, using full-field displacements obtained from the digital image correlation technique is presented. Surface displacements and strains during the fracture test of notched SFRC beams with volume fractions (V_f) of steel fibers equal to 0.5 and 0.75% are analyzed. An analysis procedure for determining the crack opening width over the depth of the beam during crack propagation in the flexure test is presented. The crack opening width is established as a function of the crack tip opening displacement and the residual flexural strength of SFRC beams. The softening in the post-peak load response is associated with the rapid surface crack propagation for small increases in crack tip opening displacement. The load recovery in the flexural response of SFRC is associated with a hinge-type behavior in the beam. For the stress gradient produced by flexure, the hinge is established before load recovery is initiated. The resistance provided by the fibers to the opening of the hinge produces the load recovery in the flexural response.

Keywords: steel fibers, toughness, crack opening, post cracking response, softening, fracture, digital image correlation.

1. Introduction

The use of steel fibers as discrete structural reinforcement in concrete has been explored and even recommended in some codes of practice. Considerable research has been performed on the fracture behavior of steel fiber reinforced concrete (SFRC). Available information suggests that while there is a nominal increase in flexural strength compared to plain concrete there is a significant increase in toughness (Gopalaratnam et al. 1991; Gopalaratnam and Gettu 1995; Armelin and Banthia 1997; Barros and Figueiras 1999; di Prisco et al. 2009; ACI 544.1R-96 2006). In SFRC, fibers enhance the post-cracking behavior by providing crack bridging stresses and thus ensure stress transfer across the cracked sections (Tadepalli et al. 2015; Sorensen et al. 2014). Several factors that influence the crack formation and crack growth include, type of fibers, volume of fibers, the distribution and orientation of fibers at the crack location (Gettu et al. 2005; Laranjeira et al. 2012; Michels et al. 2013; Islam and Alam 2013; Abdallah et al. 2016; Adjrad et al. 2016).

An understanding of the contribution of these fibers in providing resistance to crack propagation and controlling crack opening has been developed by combining fracture mechanics-based approaches with local information provided by the high resolution experimental techniques. Optical techniques such as speckle pattern interferometry and Moire interferometry have been used to investigate the fracture process zone in concrete and fiber reinforced concrete (Shah and Ouyang 1991). The information from these techniques has been used primarily to evaluate the localization and toughening mechanisms. The high resolution optical techniques provide information within a limited field of view. The information from the local measurement is then applied to a numerical or analytical framework to relate the local material behavior with the global response. Digital image correlation (DIC) has emerged as a full-field optical technique, which provides adequate resolution of the local strains close to the crack tip while providing far-field information. DIC has been applied successfully to obtain the cohesive interface fracture behavior of the FRP-concrete bond (Ali-Ahmad et al. 2006; Subramaniam et al. 2007; Carloni and Subramaniam 2010, 2013; Carloni et al. 2012). Limited number of application of DIC technique for studying the crack growth in fiber reinforced concrete have also been attempted (Robins et al. 2001; Subramaniam et al. 2015).

Several analytical formulations with different levels of approximations have been proposed for predicting the load response of concrete considering its post-cracking behavior. In most representations, the behavior of the crack and the fracture process zone is idealized within the geometric relations imposed by geometry and loading (Hillerborg et al. 1976; ACI 544.8R 2016). A convenient idealization of the facture behavior of concrete is the cracked hinge model, where a hinge-type behavior is postulated for predicting the response of concrete in flexure (Stang and Olesen 1998;

Department of Civil Engineering, Indian Institute of Technology Hyderabad, Hyderabad 502285, India.
*Corresponding Author; E-mail: kvls@iith.ac.in

Published online: 19 May 2017

Olesen 2001). The non-linearity caused by the presence of crack is assumed to be confined within a hinge region of finite width and the stress bridging across the crack are considered in the form of a stress-crack separation relationship. The hinge is connected to elastic beams at each end and the stress state in the elastic beam is the far-field stress given by the elastic beam theory. While the idealization provides adequate prediction of load response, direct validation of the hinge-type behavior is not yet available.

The focus of this paper is to study the crack propagation using a high resolution full-field optical technique, which provides sufficient accuracy of the local strain localization behavior and sufficient full-field view to allow the study of far-field response. An experimental investigation into the flexural response of notched SFRC beams is presented, where insights into the crack propagation and post-cracking response in the composite are obtained using DIC. Insights into crack propagation and the post cracking response are obtained by combining information from both the near-field and far-field measurements. The surface displacements and strains are analyzed for evaluating the crack growth in concrete in relation to the observed load response in flexure. The measured crack opening at the tip of the notch obtained from the DIC measurement is compared with the crack tip opening displacement obtained using a surface mounted gauge. The influence of fibers at the different points of the flexural load response is evaluated in relation to the measured crack length and profile.

2. Materials and Methods

Commercially available ordinary Portland cement confirming to the requirements Grade 53 of Indian standard, IS 12269 with specific gravity of 3.1 and fineness modulus of 325 m^2/kg was used for all concrete mixtures. Siliceous fly ash conforming to the requirements of IS 3812-1 (2003) and IS 1727 (1967) with specific gravity of 2.5 and fineness modulus of 320 m^2/kg was used as supplementary cementitious material in concrete mixtures. Crushed sand with a specific gravity of 2.67 and fineness modulus of 2.83 was used as fine aggregate and crushed granite of specific gravity of 2.63 was used as coarse aggregate. Two different coarse aggregate fractions with maximum size in ranges of 10–4.75 mm and 20–10 mm were blended in equal proportions for use in the concrete mix.

The cementitious content of the concrete mix was fixed at 340 and 140 kg/m^3 fly ash was used. The water-to-cementitious ratio equal to 0.48 and was kept constant in all mixes. In the concrete mixture fine aggregates were taken as 45% of the total aggregate volume fraction. One control mixture and mixtures with different dosage of hooked end steel fibers were prepared from one batch of ingredients. The control mixture contained no fiber. Fiber reinforced concrete (FRC) mixtures were prepared with fiber volume fractions (V_f) equal to 0.50 and 0.75% and are labelled as SFRC50 and SFRC75, respectively.

150 mm Cubes and beams with dimensions 150 mm (height) × 150 mm (width) × 500 mm (length) were cast from each mixture. Concrete was prepared using a drum mixer with a capacity of 0.25 m^3. The ingredients were put into the mixer in the decreasing order of sizes starting from 20 mm coarse aggregate to cement. Dry mixing of the aggregates and cement was done for 2 min and then water was added gradually in the rotating mixer and allowed to mix for 5 min. During the mixing process, the walls and bottom of mixer were scraped well to avoid sticking of mortar. Super plasticizer (Gelenium) was used to increase the workability of freshly prepared fiber reinforced concrete. A consistent slump in the range 75–100 mm was maintained for all mixtures. Finally, the fresh concrete was placed in oiled moulds and compacted properly in three layers, each layer being tamped 35 times using a tamping rod and compacted using needle vibrator. After the initial setting of concrete, the surface of the specimen was finished smooth using a trowel. Immediately after casting, all specimens were covered with wet burlap and plastic covers to minimize moisture loss and stored room temperature, approximately 25 °C. Specimens were demolded 24 h after casting and stored under water up to 28 days of age.

The 28-day compressive strengths obtained from the 150 mm concrete cubes of the different mixtures evaluated in this study are given in Table 1. An increase in the compressive strength with increasing fiber volume in SFRC is observed.

2.1 Three-Point-Flexure Test

The test procedure adopted was consistent with the guidelines given in EN 14651:2005 and consisted of testing prismatic specimens in a three-point bending configuration. Specimens were rotated 90° along the longitudinal axis so that casting surface was on the back side during the flexure test and a notch of 25 mm depth was introduced at the mid-span using a circular saw as per the guidelines given in EN 14651:2005. The flexure test was conducted in crack mouth opening displacement (CMOD) control. The loading fixture conformed to the requirements of EN 14651:2005. The corresponding deflection of the beam was measured using the rectangular jig clamped to the specimen at mid-depth directly over the supports. During the test, the crack tip opening displacement (CTOD) was also measured using a clip gauge mounted at the tip of the notch. A schematic sketch of the test setup is shown in Fig. 1. The notched beam was tested with a span equal to 450 mm. The rate of increase of the CMOD during the flexure test was controlled in two stages, at 0.05 mm/min for CMOD less than 0.1 mm and at

Table 1 Cube compressive strengths of concrete mixtures.

Specimen	Mean compressive strength (MPa)	SD (MPa)
Control	34.6	1.05
SFRC50	34.4	0.82
SFRC75	40.4	1.88

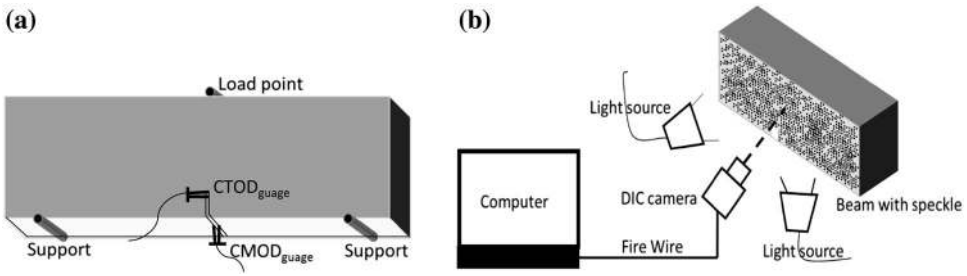

Fig. 1 Experimental setup for flexure test of notched specimens: **a** schematic sketch showing the placement of gauges; **b** schematic representation of the DIC setup for obtaining images from the front face during flexure test.

0.1 mm/min for CMOD greater than 0.1 mm. All the tests were ended when the CMOD reached a value of 4 mm. Six specimens were tested for each concrete mixture.

2.2 Digital Image Correlation

For the use in image analysis, a sprayed-on speckle pattern was created on the surface of the beam in a region close to the notch. A uniform coat of white paint was applied of the surface to provide a uniform background. The sprayed-on speckle was created by spraying a black mist. During the flexure test, digital images of the specimen were captured using a high resolution camera (5 mega pixels). Uniform light intensity was ensured across the surface of the cube using normal white light. The camera was fitted with a 50 mm lens and was placed at a distance of 1 m from the specimen surface. Calibration for the pixel size was performed using a graduated rule placed in front of the specimen. From this measurement, the physical calibration was established and was in the range of 12–14 pixels per mm. A reference image was captured in the undeformed state prior to the initiation of loading program. Images of the specimen were captured at regular intervals during the test.

DIC is a method based on digital image analysis, which provides full-field, spatially continuous measurement of displacements across the surface of the specimen. The surface displacements are obtained from correlation of the random pattern of speckles between images of the specimen undergoing deformation and the specimen in the reference (undeformed) configuration. The speckle pattern represents a random pattern, which gives a unique distribution of pixel gray level values. A two-dimensional displacement field was obtained for all points on the surface from cross-correlating the image of the deformed specimen with the image of the specimen in the reference configuration. Correlations and pattern identification is performed within small neighborhoods called subsets (Sutton et al. 1983, 1988; Pan et al. 2009). In a given image, the pixel gray-levels in each subset associated with the random sprayed-on pattern gives a unique gray-level pattern, which differs from gray-level distribution in another subset. In the analysis, positions within the deformed image were mapped on to positions within the reference subsets using second-order, two-dimensional shape functions. Spatial domain cross-correlation was performed to establish correspondence between matching subsets in images of the reference and the deformed states. Quintic B-spline interpolation of the gray values was used to achieve sub-pixel accuracy. The cross correlation analysis which maximizes the correlation coefficient between gray levels in the subsets in the reference and deformed images of the digital images was performed using the VIC-2D^{TM} software. Surface displacements and displacement gradients at each loading stage were calculated at each subset center, by evaluating the shape functions and their partial derivatives at the center of the subset. For the setup used in this study, the random error in the measured displacement is in the range of 0.002 pixels. Strains were computed from the gradients of the displacements.

3. Results

The load-CMOD responses of the control and the SFRC specimens are shown in Fig. 2a. The load-CMOD response close to the peak is shown in Fig. 2b. There is an increase in the peak load (identified as F_L, the load corresponding to limit of proportionality (LOP) as per EN 14651:2005) with increasing V_f. There is softening in the load response immediately following the F_L. In FRC specimens there is an increase in the load carrying capacity with increasing crack opening after the softening load response. The load recovery is initiated at a smaller value of crack opening displacement and a higher load is achieved during the load recovery on increasing the V_f. The increase in the residual load carrying capacity with increasing CMOD indicates that the steel fibers are effective in providing crack closing stresses with increasing crack opening.

The F_L and corresponding CTOD from the control and the SFRC specimens are tabulated in Table 3. The load in the post-peak at which load recovery is initiated, identified as F_{crit}^{CTOD} and the corresponding CTOD, identified as $CTOD_{crit}$ are also tabulated in Table 2. There are systematic changes in all values with an increase in the fiber volume content and

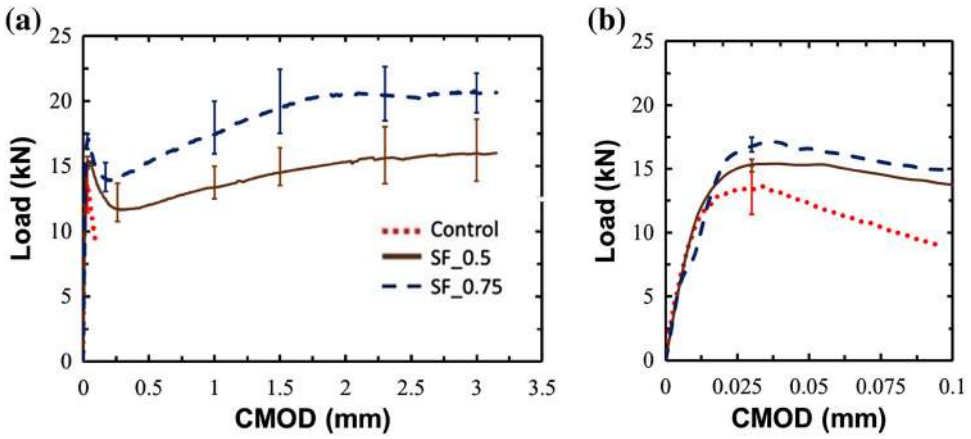

Fig. 2 Load-CMOD response from flexure tests **a** up to a CMOD = 3 mm; and **b** early response up to CMOD = 0.1 mm. The average response of five beams is plotted with *scatter bars* indicating the range of variation at discrete values of CMOD.

Table 2 Load and CTOD measures from tests on notched beam.

Fiber type	Vol. %	F_L (SD) kN	CTOD at peak load (SD) μm	Mean F_{crit}^{CTOD} (stdev) kN	Mean $CTOD_{crit}$ (SD) μm
Control		13.8 (1.44)	22 (6.5)		
SFRC50	0.5	15.92 (0.67)	28.5 (6.25)	11.54 (1.2)	257 (33.6)
SFRC75	0.75	17.03 (0.86)	25.1 (4.52)	13.77 (1)	174 (10.6)

the observed change in the mean values are outside the range of scatter obtained from one group. The $CTOD_{crit}$ provides a qualitative measure of the crack opening when the load recovery is initiated. Increasing the fiber volume content increases the resistance to crack opening, thereby resulting in an earlier deviation from the descending portion of the load response seen in control specimens. Thus, at larger volume fractions, the fibers are effective at a smaller crack opening. The available data indicates that load recovery is initiated after a CTOD value of 250 μm and 175 μm for 0.5 and 0.75% fiber volume contents, respectively.

The results of the notched tests were analyzed using the procedure given in of UNI 11039-2. The first crack flexural strength (f_{If}), equivalent flexural strengths ($f_{eq(0-0.6)}$, $f_{eq(0.6-3)}$) were evaluated. In the current study the flexural tests on notched beams were performed as per EN 14651 (2005), which recommends a three-point bending configuration. The UNI 11039-2 standard formulae were developed for four-point bending configuration. The first crack nominal strength, f_{If} and the equivalent flexural strengths were calculated using modified formulae, where a factor of 1.5 was introduced as shown below.

Table 3 Strength values as per UNI 11039-2.

	F_L (kN)	f_{If} (MPa)	$f_{eq(0-0.6)}$ (MPa)	$f_{eq(0.6-3)}$ (MPa)
Control	13.78	3.97	–	–
SFRC50	15.89	4.57	3.12	19.02
SFRC75	17.48	5.04	3.67	22.72

$$f_{If} = \frac{1.5 \cdot F_L \cdot l}{b \cdot (h - a_0)^2} (\text{MPa}), \tag{1}$$

$$f_{eq(0-0.6)} = \frac{1.5 \cdot l}{b \cdot (h - a_0)^2} \cdot \frac{U_1}{0.6} (\text{MPa}), \tag{2}$$

$$f_{eq(0.6-3)} = \frac{1.5 \cdot l}{b \cdot (h - a_0)^2} \cdot \frac{U_2}{2.4} (\text{MPa}), \tag{3}$$

where b (150 mm), h (150 mm), l (450 mm) and a_0 (25 mm) are the width, the length, the height and the notch length, respectively. U_1 and U_2 are given by the area under load-CTOD (F(CTOD)) response as shown below

$$U_1 = \int_0^{0.6} F(CTOD) \cdot d(CTOD), \tag{4}$$

$$U_2 = \int_{0.6}^{3} F(CTOD) \cdot d(CTOD). \tag{5}$$

The equivalent flexural strengths for the control and the SFRC beams are shown in Table 3. It can be seen that there is an increasing trend in the first crack strength with increasing fiber content. The values of $f_{eq(0-0.6)}$ and $f_{eq(0.6-3)}$ show clear improvement on increasing the V_f from 0.5 to 0.75%.

3.1 Results of Digital Image Analysis

Contours of strain in the X-direction (ε_{xx}) at distinct points on the load response of an SFRC50 specimen are shown in Fig. 3. A subset size of 35 pixels was used for the analysis. The load points are identified on the load-CMOD response of the specimen in Fig. 3a. The ε_{xx} at progressively larger

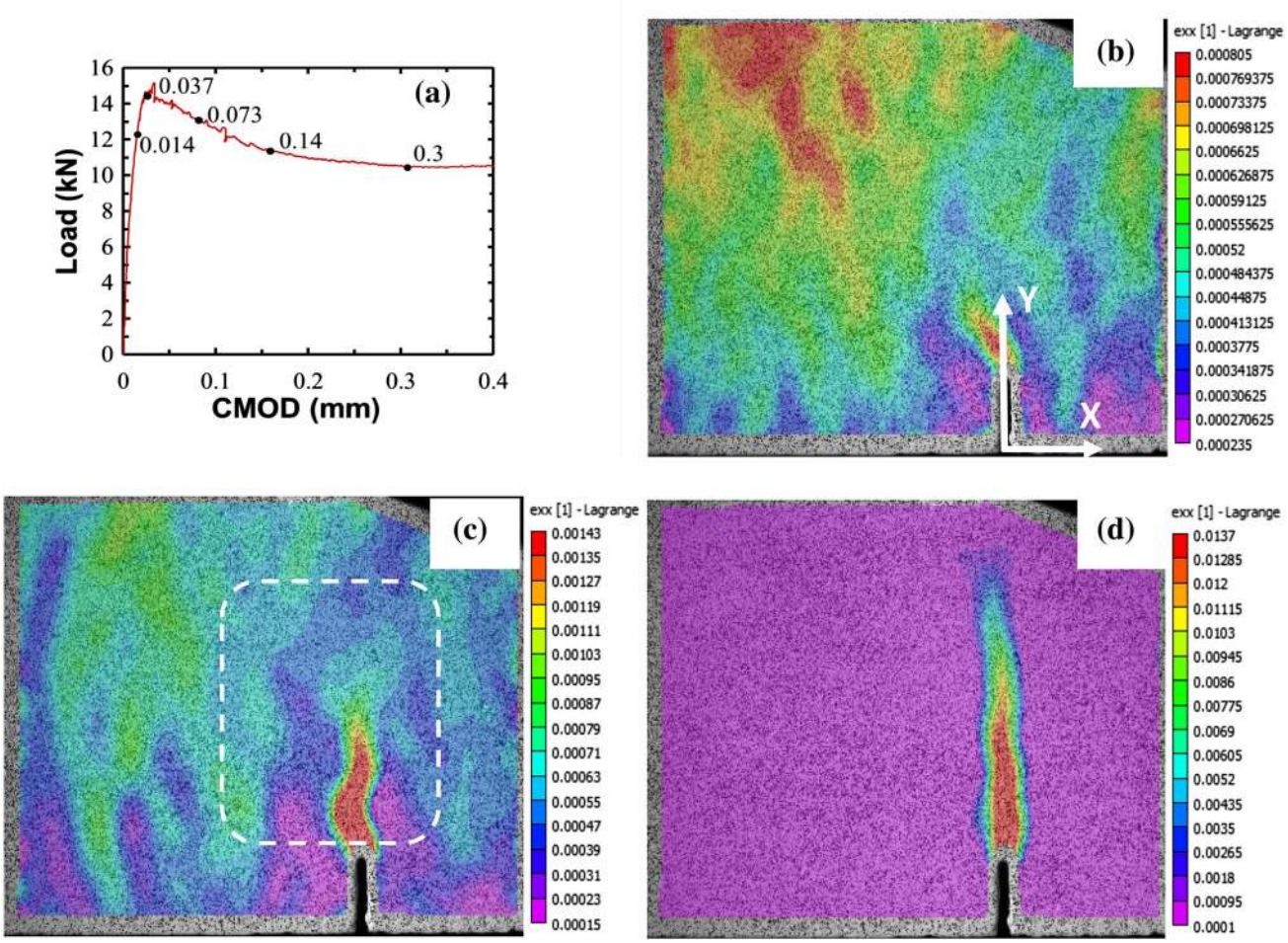

Fig. 3 **a** Load CMOD response of SFRC specimen with $V_f = 0.5\%$; Contours of ε_{xx} at **b** Load Point 1 (CMOD = 0.014 mm); **c** Load Point 2 (CMOD = 0.037 mm), **d** Load Point 5 (CMOD = 0.3 mm).

values of CMOD are shown in Figs. 3b–d. Strain localization is evident in the pre-peak load response and with increasing CMOD, leads to the formation of a single crack emanating from the notch. The increase in the crack length can clearly be identified with softening in the post peak load response; as the crack propagates, there is a steady increase in the crack opening and an associated decrease in the load. The physical opening produced by the crack emanating from the notch resulted in a loss of correlation within a region corresponding to the subset size used for correlation centered on the location of the crack.

The contours of displacement in the X-direction, U_x at the load point with CMOD = 0.037 mm using different subset sizes within an area of interest located over the notch (shown marked in Fig. 3c) are shown in Figs. 4a–c. The closeness of displacement contours directly over the notch indicates localization. While using a smaller subset size results in the local variations being accurately represented, the influence of local heterogeneities in the material becomes more prominent. Since concrete is a heterogeneous material, on decreasing the subset size, the measured observations contain significant contributions of local effects on the scale of the inhomogeneity within the material. Increasing the subset size has the effect of smearing out the sharp gradients in the displacements. The subset size of 35 pixels was found to provide sufficient resolution of the local behavior close to the notch and provide adequate accuracy in the far-field measurements. A conservative estimate of the resolution in strain obtained from the digital correlation was 5 με (Bruck et al. 1989; Schreier and Sutton 2002).

The U_x, and the ε_{xx} along length of the member on a horizontal line with fixed Y coordinate located at a distance equal to 37 mm above the bottom face of the beam and 12 mm above the tip of the notch at different points in the load response (in Fig. 3a) are shown in Fig. 5. The U_x away from the notch, as X increases from −75 mm, exhibits a steady increase with the X coordinate. The stress concentration produced by the notch and subsequent crack propagation associated with increasing CTOD produce sharp gradients in U_x within a small region close to the notch (values of X close to zero). In the far-field, away from the region of high displacement gradients, U_x varies linearly with a slope which is nominally constant. The magnitudes of displacements in the far-field region are proportional to the magnitude of applied stress. The variation of ε_{xx} with X, along the line shows a sharp increase in the magnitude of strains to values significantly higher than the far field values within the region of large displacement gradient close to the notch, indicating localization of strain. There is an increase in the magnitude of strain and there is also a sharper strain

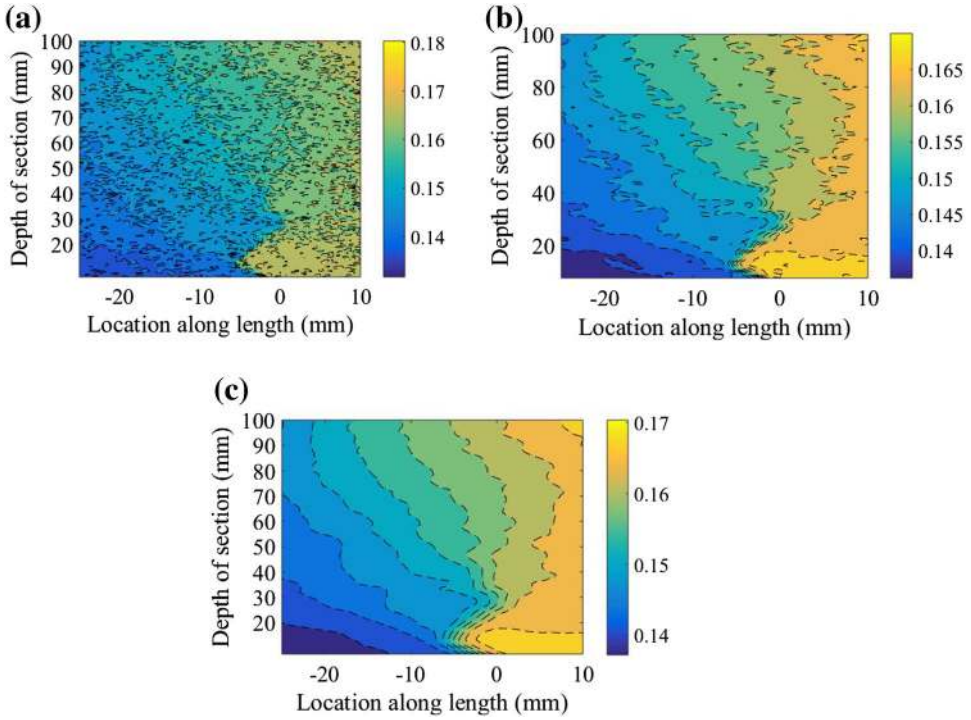

Fig. 4 Contours of U_x at CMOD = 0.037 mm corresponding to different subset sizes: **a** subset size of 15 × 15 pixels; **b** subset size of 35 × 35 pixels; **c** subset size of 75 × 75 pixels.

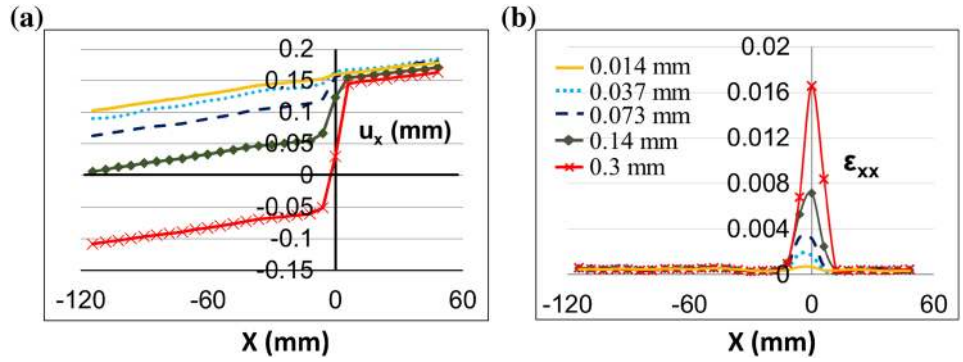

Fig. 5 Variation of U_x and ε_{xx} with varying X located at Y = 37 mm in SFRC specimen with V_f = 0.5% (load response shown in Fig. 3): **a** U_x with X; **b** ε_{xx} with X for different values of CMOD.

gradient within the region of localization with increasing CTOD.

The correlation coefficient at load points with CMOD values equal to 0.3 mm, are shown in Fig. 6. The physical contour of the crack can be identified by the region with a loss of correlation. The physical separation in the material, produces a loss in correlation, which occurs within subsets which overlap with the opening. From the physical calibration, the width of the region associated with the loss of correlation is approximately 0.4 mm. The correlations outside the region disturbed by the crack were found to be within limits of acceptability.

The effect of the finite subset size is to smear out the sharp strain gradients. The influence of local areas where correlations are poor are also included in the local values of strain. The available resolution from the DIC technique, considering the finite subset size does not allow for determining fracture parameters using local displacement and strain measurements in regions with a physical crack. A procedure

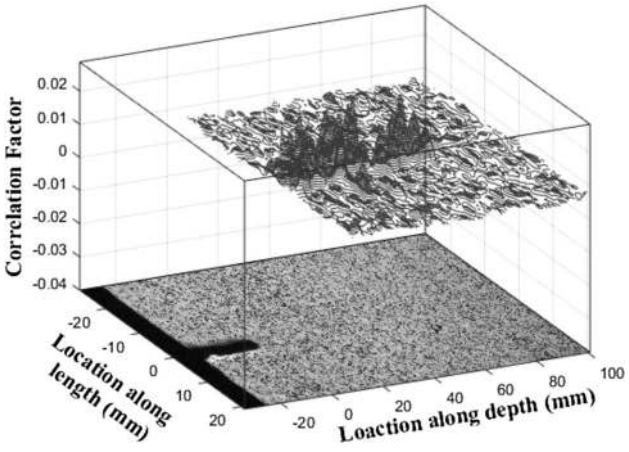

Fig. 6 Contours of correlation coefficient at Load Point 5 (CMOD = 0.3 mm).

using asymptote matching of the far-field displacements was developed to estimate the displacement discontinuity associated with crack opening, which does not rely on local measurements in regions overlapping with the crack as shown in Fig. 7. The 3D contours of U_x obtained at Load Point 5 (CMOD = 0.3 mm) are shown in Fig. 7a. The sharp gradient in U_x is introduced by the crack emanating from the notch. The asymptotic behavior in the displacement profile with the X coordinate along a line of constant Y coordinate is the far-field displacement associated with flexure. Slopes of the lines on either side of the localization region were determined by fitting straight line equations (linear equation with constant slope) to the far-field displacements on either side of the notch using least squares approximation. The slopes of the two lines obtained from the linear fits to the variation in the far-field displacement with X coordinate were found to be nominally equal. The increment in the displacement within the region of localization, which represents the displacement discontinuity introduced by crack was determined as the difference in the values of the intercepts on the Y axis of the two lines fitted to the far-field displacements. The displacement discontinuity along a line of constant Y coordinate (at a given location above the notch) determined using the procedure described above is referred to as crack opening width (Shown in Fig. 7b).

Horizontal lines spaced at 80 pixels (approximately 6.0 mm spacing), located at different depths relative to the notch, were used to obtain the crack opening width along the depth of the beam. Crack opening widths were obtained at different points on the load response. The area of interest selected for correlations passes a few millimeters over the notch. The exact location of the tip of the notch was approximated using gray scale thresholding of pixel intensities in the digital images of the specimen. From the gray scale image of the notched specimen in the reference state, the machine cut notch profile was identified using a pixel intensity value equal to 10 on a grayscale intensity scale of 256. For lines with constant Y coordinate, the tip of the notch was located as the position along Y where the threshold was not exceeded on traversing along X coordinate.

The crack opening widths along the depth of a control specimen at different values of CTOD are shown in Fig. 8. The crack opening width exhibits a decreasing profile with increasing height above the notch (increasing Y coordinate). Initially, for small values of CTOD, the crack opening width rapidly approaches a value of zero with increasing Y, away from the notch. A crack opening width equal to zero indicates that displacement profile does not show localized increase in displacement; the asymptotic displacement profiles intercept the Y axis at the same location, with no jump. At this location, the displacement profile may be assumed to be given by the far-field stress and the influence of the notch or crack is insignificant. The available data suggests that initially, the point of zero crack opening advances rapidly along the depth of the beam for a small increment in the CTOD. The point of zero crack opening progresses to a depth in the range 110–120 mm very rapidly with increasing CTOD between 0.035 and 0.082 mm. This occurs in the post peak softening load response immediately following the peak load. On increasing the CTOD further, while the crack opening width indicates a wider opening along the depth, the point of zero crack opening width remains relatively stationary. The opening of the crack therefore exhibits a hinge-type behavior, as the crack opens about a fixed point along the depth of the beam.

The observed crack opening width as a function of depth with increasing CTOD can be interpreted in terms of crack growth in the specimen. The rapid progression of the location of the zero crack opening along the depth of the beam is indicative of crack propagation. The initial growth corresponds with the pre-peak and the immediate post-peak part of the load response. In the initial growth period, there is a very rapid increase in crack length along the depth of the beam associated with a small increase in CTOD. With increasing CTOD, the crack advances to a depth of 110–120 mm, following which there is little or no change in the location of the zero crack opening width. There is however a continuous increase in the crack opening width along the depth of the crack with increasing CTOD. This experimental observation indicates

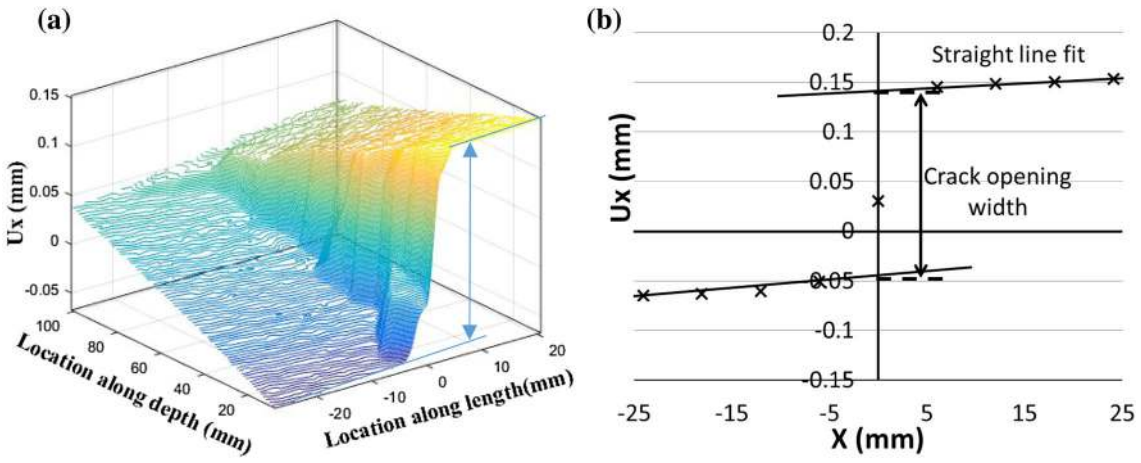

Fig. 7 **a** A 3-D representation of the displacement discontinuity introduced by the crack emanating from the notch; **b** Asymptote matching procedure for determining the crack opening displacement.

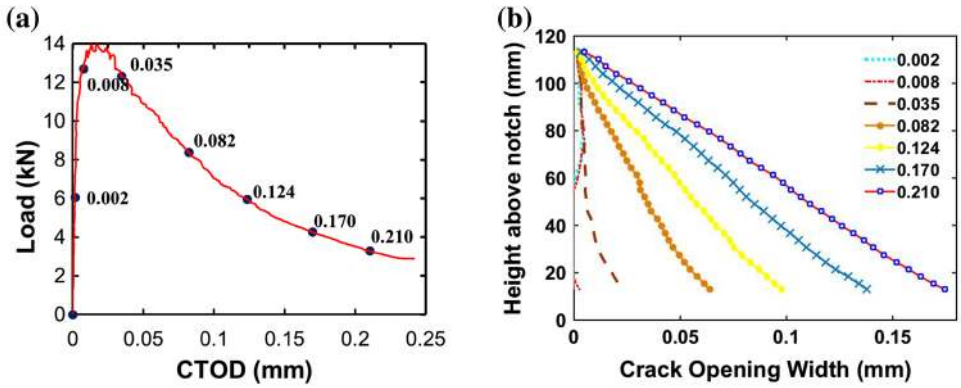

Fig. 8 **a** Load-CTOD response of a control specimen; **b** Crack opening width as a function of height above the notch for different values of CTOD.

the formation of a hinge along the depth of the beam. After formation of the hinge there is a continuous opening of the crack about a fixed location along the depth of the beam. The subsequent load response is therefore governed by the stress transfer across the crack. For control specimen, the opening of the crack leads to a continuous decrease in the load carrying capacity.

A validation of the crack profile in the beam determined using DIC was attempted using the measured crack tip opening displacement (CTOD) as a reference. The CTOD was measured at the tip of the notch using the surface mounted clip gauge, which was precisely attached at the tip of the notch. The CTOD from the DIC measurement was determined by extrapolating the crack opening width vs depth line to zero depth (the tip of the notch) and is referred to as $CTOD_{DIC}$. The extrapolation was performed by fitting a line using a least square approximation to the points located within 30 mm from the bottom of the area of interest used for image correlation. This corresponds to data from five equi-spaced lines located 6 mm apart, which were used for generating the crack width profile. The $CTOD_{DIC}$ values were obtained for different images captured at different values of CTOD. A comparison of the load-CTOD response obtained from the physical measurement using the surface mounted LVDT and that obtained from DIC measurements is shown in Fig. 9. The response obtained using both CTOD and $CTOD_{DIC}$ show a good match, which provides validation for the methodology for establishing crack profile width using image analysis.

The crack opening widths as a function of depth for different values of CTOD for an SFRC50 and an SFRC75 specimens are shown in Figs. 10 and 11 respectively. The response is nominally similar to that observed in control specimens. There is a rapid upward movement in the location of the zero crack opening width in the softening part of the load response immediately after the peak load. A rapid advance to a depth 110–120 mm above the notch, occurs up to crack opening displacements, which coincides with the initiation of the load recovery. The load recovery portion is associated with opening of the crack, with insignificant crack advance. The crack therefore develops a

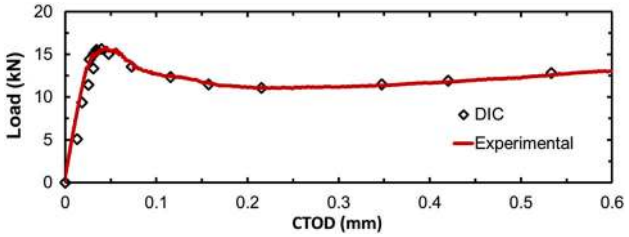

Fig. 9 Comparison of $CTOD_{DIC}$ and CTOD measured using surface mounted clip gauge.

hinge-type mechanism, where the equilibrium is maintained by the stress transfer across the crack provided by the fibers. For FRC specimen, the opening of the crack associated with the hinge action leads to an increase in the load carrying capacity. The results indicate that the crack propagation in the matrix predominantly occurs in the post-peak softening response immediately following the peak load. The fibers provide resistance to opening of the hinge, once it is established. The resistance to crack opening which contributes to the opening of the hinge is due to pullout of fibers from the matrix.

A plot of the crack extension in relation to the CTOD is plotted in Fig. 10. The physical crack tip was located based on the correlation values exceeding a threshold value following a procedure established previously (Carloni and Subramaniam 2010). The average value of correlation obtained from a region away from the crack located in regions $X < -20$ mm and $X > 20$ mm was used as the threshold value, which was found to be 0.0015. The region selected for obtaining the reference for the threshold value was sufficiently removed from the crack to provide a representative value for the correlation index within the specimen. Using this criterion, the physical location of the crack tip can be estimated to within the size of one subset. Depth of crack thus calculated for different images is plotted with against the corresponding CTOD in Fig. 12. The results confirm that initially there is a very rapid extension of crack for very small increase in crack opening. Subsequently, once the hinge is established, there is very small increment in the

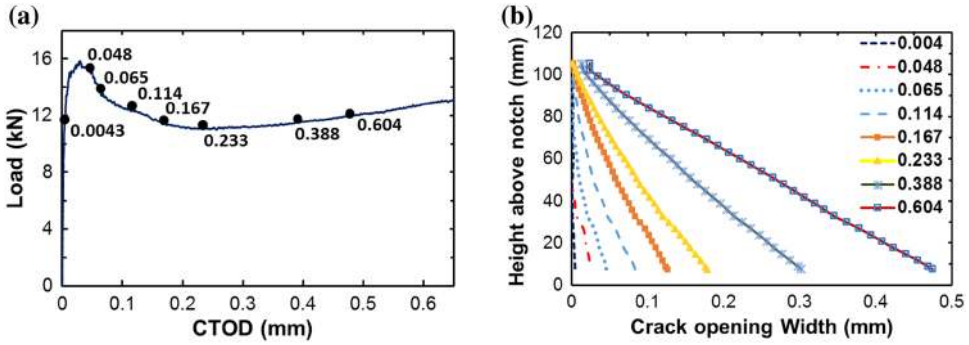

Fig. 10 Results from an SFRC50 specimen: **a** load-CTOD response of a typical specimen; **b** crack opening width as a function of height above the notch for different values of CTOD (in mm).

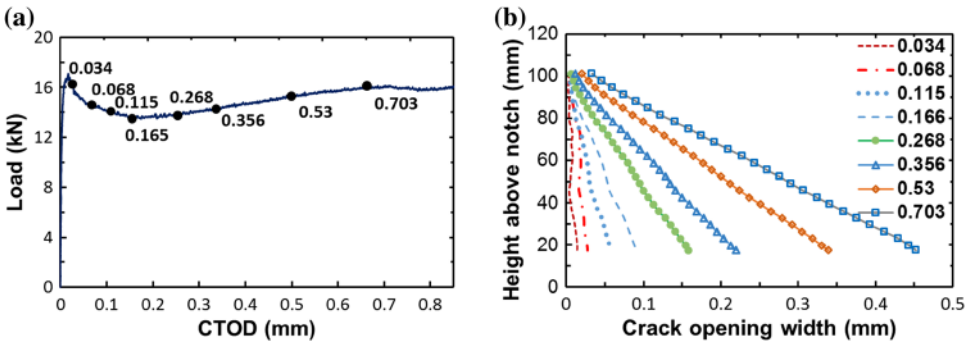

Fig. 11 Results from an SFRC75 specimen: **a** load-CTOD response of a typical specimen; **b** crack opening width as a function of height above the notch for different values of CTOD (in mm).

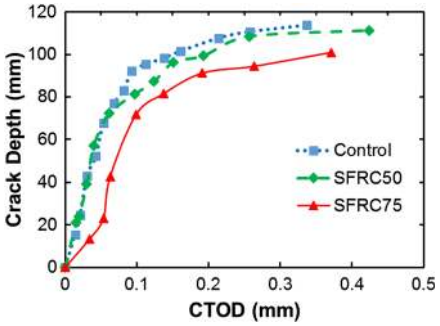

Fig. 12 Depth of crack extension with CTOD for control, SFRC50 and SFRC75.

crack depth for a large increase in crack opening. The influence of steel fibers at 0.5% V_f produce a deviation in the response once the crack advances to a depth of 70 mm, which occurs close to the peak flexural load. This relates to the small increase in the peak load in the flexural test response. At higher V_f equal to 0.75%, there is a significant difference in the crack depth at all values of CTOD. There is therefore a significant difference in the peak load and the subsequent flexural test response.

4. Summary and Findings

The available information from the different test techniques can now be combined to gain an insight into the crack propagation and opening in steel fiber reinforced concrete in flexure. Crack propagation in the FRC specimens is primarily associated with the decreasing load in the post-peak region immediately following the peak load. An asymptote matching procedure which uses the far-field displacements to estimate the displacement discontinuity produced by a crack was developed. In this procedure the inaccuracies in the local measurements at the crack location introduced by the finite subset size and the lack of correlation due to the physical opening of the crack are not considered. Subsequent load recovery in flexural load response of SFRC beams is due to hinge action associated with pullout of fibers. The available information from DIC agrees with the standard test measures of $f_{eq(0-0.6)}$ obtained from UNI 11039. $F_{eq(0-0.6)}$ provides a measure of energy in the early part of the post peak, which is associated with hinge formation and initial opening of the hinge. The $f_{eq(0.6-3)}$ value is indicative of the energy dissipated in pullout of fibers in a part of the load response which is associated with opening of the hinge.

The findings of the experimental investigation are summarized below.

1. In SFRC loaded in flexure, the surface crack propagates rapidly through the depth of the specimen for small crack openings. For V_f up to 0.75%, the resistance provided by steel fibers during the crack propagation stage is insufficient to prevent a softening in flexure. The fibers do influence the peak load and the rate of softening in post-peak produced by crack propagation.
2. Fiber volume content plays a significant role in improving the load recovery in the post-peak flexural

response, which contributes to increasing toughness. The load recovery is associated with a hinge type behavior. For the stress gradient produced by flexure, the hinge is established at a crack tip opening displacement before load recovery is initiated. After the formation of a hinge, the resistance to the crack opening is attributed to fiber pullout from the cementitious matrix. The recovery is initiated with sufficient number of fibers crossing the crack, which provide the required resistance across the surface of the crack.

3. At fiber volume content equal to 0.75% there is a significant decrease in the crack depth for a given crack tip opening displacement. This produces significant improvements in the peak load and the post peak load resistance response in flexure.

Acknowledgements

The authors would like to acknowledge support of the Center of Excellence in Sustainable Development at I.I.T. Hyderabad, funded by the Ministry of Human Resource Development, India.

Open Access

References

544.1R-96. (2006). *Report on fiber reinforced concrete*. Farmington Hills, MI: American Concrete Institute.

544.8R-16. (2016). *Report on indirect method to obtain stress-strain response of fiber-reinforced concrete (FRC), ACI Committee 544 ACI 544.8R*. Farmington Hills, MI: American Concrete Institute.

Abdallah, S., Fan, M., Zhou, X., & Le Geyt, S. (2016). Anchorage effects of various steel fibre architectures for concrete reinforcement. *International Journal of Concrete Structures and Materials, 10*(3), 325–335.

Adjrad, A., Bouafia, Y., Kachi, M. S., & Ghazi, F. (2016). Prediction of the rupture of circular sections of reinforced concrete and fiber reinforced concrete. *International Journal of Concrete Structures and Materials, 10*(3), 373–381.

Ali-Ahmad, M., Subramaniam, K., & Ghosn, M. (2006). Experimental investigation and fracture analysis of debonding between concrete and FRP sheets. *Journal of engineering mechanics, 132*(9), 914–923.

Armelin, H. S., & Banthia, N. (1997). Predicting the flexural postcracking performance of steel fiber reinforced concrete from the pullout of single fibers. *ACI Materials Journal, 94,* 18–31.

Barros, J. A., & Figueiras, J. A. (1999). Flexural behavior of SFRC: Testing and modeling. *Journal of Materials in Civil Engineering, 11*(4), 331–339.

Bruck, H. A., McNeill, S. R., Sutton, M. A., & Peters, W. H. (1989). Digital image correlation using Newton-Raphson method of partial differential correction. *Experimental Mechanics, 29*(3), 261–267.

Carloni, C., & Subramaniam, K. V. (2010). Direct determination of cohesive stress transfer during debonding of FRP from concrete. *Composite Structures, 93*(1), 184–192.

Carloni, C., & Subramaniam, K. V. (2013). Investigation of subcritical fatigue crack growth in FRP/concrete cohesive interface using digital image analysis. *Composites Part B Engineering, 51,* 35–43.

Carloni, C., Subramaniam, K. V., Savoia, M., & Mazzotti, C. (2012). Experimental determination of FRP–concrete cohesive interface properties under fatigue loading. *Composite Structures, 94*(4), 1288–1296.

Di Prisco, M., Plizzari, G., & Vandewalle, L. (2009). Fibre reinforced concrete: new design perspectives. *Materials and Structures, 42*(9), 1261–1281.

EN 14651:2005 (E). (2005). *Test method for metallic fibre concrete. Measuring the flxural tensile strength (limit of proportionality (LOP), residual).*

Gettu, R., Gardner, D. R., Saldivar, H., & Barragán, B. E. (2005). Study of the distribution and orientation of fibers in SFRC specimens. *Materials and Structures, 38*(1), 31–37.

Gopalaratnam, V. S., & Gettu, R. (1995). On the characterization of flexural toughness in fiber reinforced concretes. *Cement & Concrete Composites, 17*(3), 239–254.

Gopalaratnam, V. S., Shah, S. P., Batson, G., Criswell, M., Ramakishnan, V., & Wecharatana, M. (1991). Fracture toughness of fiber reinforced concrete. *Materials Journal, 88*(4), 339–353.

Hillerborg, A., Modéer, M., & Petersson, P. E. (1976). Analysis of crack formation and crack growth in concrete by means of fracture mechanics and finite elements. *Cement and Concrete Research, 6*(6), 773–781.

IS 1727. (1967). Methods of test for pozzolanic materials [CED 2: Civil Engineering], Bureau of Indian Standards, New Delhi, India.

IS 3812-1. (2003). Specification for pulverized fuel ash, part 1: For use as pozzolana in cement, cement mortar and concrete [CED 2: Cement and concrete], Bureau of Indian Standards, New Delhi, India.

Islam, M. S., & Alam, S. (2013). Principal component and multiple regression analysis for steel fiber reinforced concrete (SFRC) beams. *International Journal of Concrete Structures and Materials, 7*(4), 303–317.

Laranjeira, F., Aguado, A., Molins, C., Grünewald, S., Walraven, J., & Cavalaro, S. (2012). Framework to predict the orientation of fibers in FRC: A novel philosophy. *Cement and Concrete Research, 42*(6), 752–768.

Michels, J., Christen, R., & Waldmann, D. (2013). Experimental and numerical investigation on postcracking behavior of

steel fiber reinforced concrete. *Engineering Fracture Mechanics, 98,* 326–349.

Olesen, J. F. (2001). Fictitious crack propagation in fiber-reinforced concrete beams. *Journal of Engineering Mechanics, 127*(3), 272–280.

Pan, B., Qian, K., Xie, H., & Asundi, A. (2009). Two-dimensional digital image correlation for in-plane displacement and strain measurement: a review. *Measurement Science & Technology, 20*(6), 062001.

Robins, P., Austin, S., Chandler, J., & Jones, P. (2001). Flexural strain and crack width measurement of steel-fibre-reinforced concrete by optical grid and electrical gauge methods. *Cement and Concrete Research, 31*(5), 719–729.

Schreier, H. W., & Sutton, M. A. (2002). Systematic errors in digital image correlation due to undermatched subset shape functions. *Experimental Mechanics, 42*(3), 303–310.

Shah, S. P., & Ouyang, C. (1991). Mechanical behavior of fiber-reinforced cement-based composites. *Journal of the American Ceramic Society, 74*(11), 2727–2953.

Sorensen, C., Berge, E., & Nikolaisen, E. B. (2014). Investigation of fiber distribution in concrete batches discharged from ready-mix truck. *International Journal of Concrete Structures and Materials, 8*(4), 279–287.

Stang, H., & Olesen, J. F. (1998). On the interpretation of bending tests on FRC-materials. In H. Mihashi & K. Rokugo (Eds.), *Fracture Mechanics of Concrete Structures* (Vol. 1). Freiburg: Aedificatio Publishers.

Subramaniam, K. V., Carloni, C., & Nobile, L. (2007). Width effect in the interface fracture during shear debonding of FRP sheets from concrete. *Engineering Fracture Mechanics, 74*(4), 578–594.

Subramaniam, K. V., Suraj, N., & Sahith, G. (2015). "Investigation of crack propagation in macro-synthetic fiber reinforced concrete." *Proc., 5th International. Conf. on Construction Materials: Performance, Innovations and Structural Implications*, 19–21 Aug.,Whistler.

Sutton, M. A., McNeill, S. R., Jang, J., & Babai, M. (1988). Effects of subpixel image restoration on digital correlation error estimates. *Optical Engineering, 27*(10), 271070.

Sutton, M. A., Wolters, W. J., Peters, W. H., Ranson, W. F., & McNeill, S. R. (1983). Determination of displacements using an improved digital correlation method. *Image and Vision Computing, 1*(3), 133–139.

Tadepalli, P. R., Dhonde, H. B., Mo, Y. L., & Hsu, T. T. (2015). Shear strength of prestressed steel fiber concrete I-beams. *International Journal of Concrete Structures and Materials, 9*(3), 267–281.

UNI 11039-2:2003. (2003). Concrete reinforced with steel fibers—test method for the determination of early crack strength and ductility indexes.